NANO LETTERS

LETTER

pubs.acs.org/NanoLett

Fully Printed Separated Carbon Nanotube Thin Film Transistor Circuits and Its Application in Organic Light Emitting Diode Control

Pochiang Chen,[†,∥] Yue Fu,[‡,∥] Radnoosh Aminirad,[†,§] Chuan Wang,[‡] Jialu Zhang,[‡] Kang Wang,[§] Kosmas Galatsis,[*,†,§] and Chongwu Zhou[*,‡]

[†]Aneeve Nanotechnologies LLC, 570 Westwood Plaza, Suite 6532, Los Angeles, California 90095, United States

[‡]Department of Electrical Engineering, University of Southern California, Los Angeles, California 90089, United States

[§]Department of Electrical Engineering, University of California at Los Angeles, Los Angeles, California 90095, United States

Supporting Information

ABSTRACT: The advantages of printed electronics and semiconducting single-walled carbon nanotubes (SWCNTs) are combined for the first time for display electronics. Conductive silver ink and 98% semiconductive SWCNT solutions are used to print back-gated thin film transistors with high mobility, high on/off ratio, and high current carrying capacity. In addition, with printed polyethylenimine with $LiClO_4$ as the gating material, fully printed top-gated devices have been made to work as excellent current switches for organic light emitting diodes (OLEDs). An OLED driving circuit composed of two top-gated fully printed transistors has been fabricated, and the successful control over external OLED is demonstrated. Our work demonstrates the significant potential of using printed carbon nanotube electronics for display backplane applications.

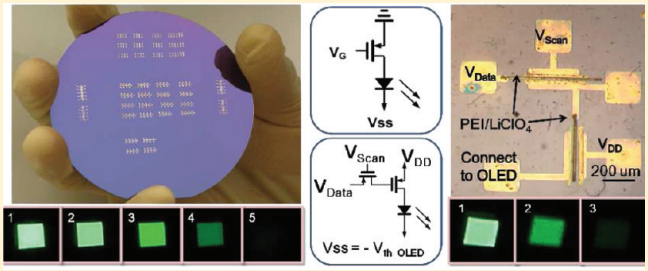

KEYWORDS: Separated semiconducting-enriched carbon nanotubes, printed electronics, display electronics, organic light emitting diode, fully printed carbon nanotube devices and circuits, thin film transistors

Since the revolutionary inventions of liquid crystal displays (LCDs) in 1964,[1,2] display electronics has undergone rapid developments and has attracted growing attention. Recently, the organic light emitting diode (OLED)[3] has shed new light on this realm. Compared to LCD, OLED has light weight, compatibility with flexible plastic substrate, wide viewing angles, improved brightness, high power efficiency, and quick response. OLED-based displays are now used in cell phones, digital cameras and other portable devices. An OLED-based flexible and rollable display prototype has also been demonstrated.[4] To allow low-cost, mass production of OLED-based displays, key issues include the materials and processes used for fabrication of OLED and driving circuit. A commercial LED/OLED-based display adopts polysilicon thin film transistor (TFT) or amorphous silicon (α-Si) TFT for compatibility with the mainstream silicon fabrication process. However, deposition of amorphous silicon and polysilicon requires a complex high-cost fabrication process. Among possible solutions, printing technology has great potential. It is a simple, low-cost, high throughput process and has been used for many electronic applications.[5−12] Plus, it is compatible with flexible substrates, making it suitable for manufacturing of OLED-based displays. While polysilicon and amorphous silicon are not compatible with printing, some organic semiconductors can be printed, but they suffer from low mobility and instability in air.

In contrast, single-walled carbon nanotubes (SWCNTs) are well-known for their high mobility, high on/off ratio, and small operation voltage.[13−15] They have been used for sensors[16−19] and digital circuits such as ring oscillators,[21−24] simple logic gates (inverters, NOR, NAND),[20−24] decoders,[20] SRAM[22] and delay flip flops (DFFs).[24] Due to the excellent current carrying capacity of SWCNTs, SWCNT TFT can provide sufficient driving current for typical high-resolution OLED displays than organic TFTs. Such advantages allow dense integration of pixels, high aperture ratio, and small power consumption. Furthermore, carbon nanotubes (CNTs) are flexible materials, and their solution is compatible with printed electronics.

The advantages of SWCNT TFTs for active matrix OLED (AMOLED) display electronics have been previously demonstrated.[25,26] However, no one has reported using SWCNT TFTs based on printing technology for display applications. In this study, we have demonstrated the first circuits composed of fully printed back-gated and top-gated SWCNT TFTs for display electronics. Our work includes the following essential components: (1) We fabricated back-gated SWCNT TFTs with high mobility (10−30 $cm^2/(V\ s)$) and high on/off ratio (10^4−10^7) purely based on printing technology. (2) With printed polyethylenimine (PEI)/$LiClO_4$ as polymer electrolyte gating material, we fabricated fully printed top-gated SWCNT TFTs with good current carrying capability. (3) We demonstrated the first fully printed single pixel OLED control circuits. Our fully printed

Received: August 10, 2011
Revised: October 17, 2011

   dx.doi.org/10.1021/nl202765b | *Nano Lett.* XXXX, XXX, 000–000

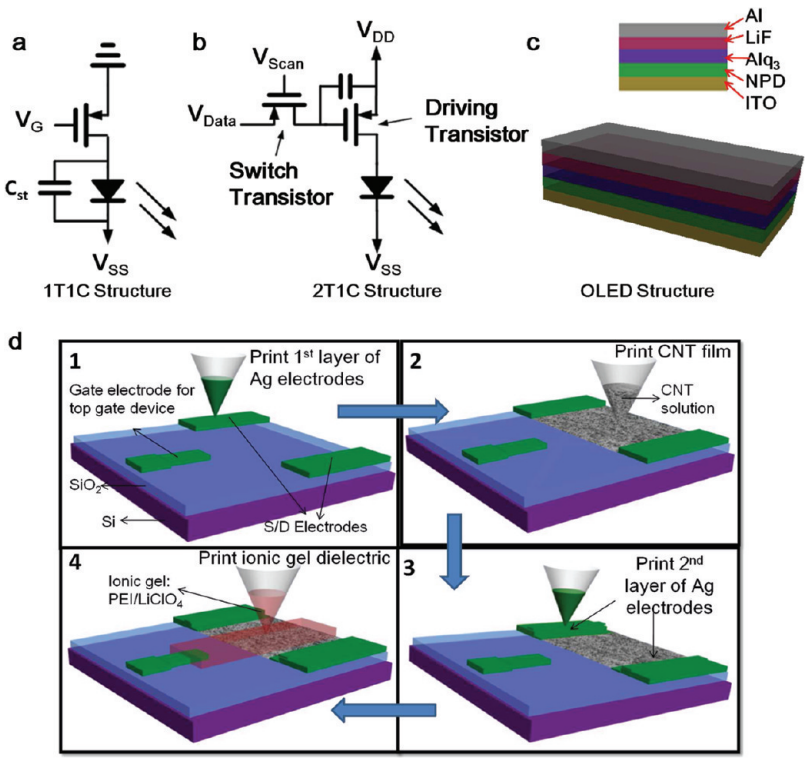

Figure 1. Schematic diagrams of typical display control circuits, OLED structure, and fabrication process of fully printed top-gated SWCNT TFT. (a) Schematic diagram of the 1T1C display control circuit. (b) Schematic diagram of the 2T1C display control circuit. (c) Cross-section view of an OLED structure. (d) Schematic diagram illustrating the fully printed back-gated and top-gated SWCNT TFT fabrication process.

SWCNT TFTs and circuits show significant advantage over traditional organic-based printed electronics with respect to stability and device performance. It suggests a practical approach for a printable, flexible OLED display and other SWCNT-based printed electronics.

Panels a and b of Figure 1 show the schematic diagrams of two typical control circuits for OLED displays, one with a single transistor and a storage capacitor (1T1C),[27] and the other with two transistors and one storage capacitor (2T1C).[28] These two circuit structures have been printed in this work without the storage capacitor and was tested with an external OLED with the structure shown in Figure 1c. Figure 1d shows the process of printing of both back-gated and top-gated SWCNT TFTs on a Si/SiO_2 wafer. Briefly, a commercial silver nanoparticle solution (Cabot Corp., CCI 300) is first printed to form source and drain electrodes, as well as gate pads to be used later for top-gated TFT structures. A postprinting sintering of the silver electrodes at 180 °C was performed to achieve small resistance (~1 Ω/sq), as was measured by the Van Der Pauw method. To improve the adhesion of SWCNT to Si/SiO_2 wafers, wafers are functionalized by diluted (aminopropyl)triethoxysilane (APTES) following our previously published recipe,[25] before printing of 98% semiconductive SWCNT solution (NanoIntegris Inc.) as the active channel material. Then the devices were rinsed with deionized (DI) water to remove the sodium dodecyl sulfate (SDS) residue after the printed SWCNT solution dried out. After inspection of the CNT film to confirm the uniformity and desired CNT density using a field emission scanning electron microscope (FESEM), another layer of silver electrodes was added along the border of silver and SWCNT film, to improve the contact between silver electrodes and SWCNT networks. Electric measurements were performed to inspect the performance of these SWCNT TFTs before printing of polymer electrolyte. Finally, $PEI/LiClO_4$ is printed as the top gate dielectric as well as gate electrode, expanding from the gate pad to the SWCNT film in the channel.

Uniformity and high density of the printed CNT film are two important issues for the printed back-gated TFTs. Panels a−c of Figure 2 show details of the as-printed back-gated SWCNT TFTs, especially for the channel region, including an optical image (Figure 2a) showing a 3-in. wafer with back-gated SWCNT TFTs with various channel widths (W) and channel lengths (L), followed by FESEM images (Figure 2b) showing the uniformity of CNT network in the channel region. A further zoomed-in FESEM image (Figure 2c) shows an approximate CNT density of 24−32 tubes/μm, which is comparable to that of previously reported SWCNT TFT work.[25,29]

Electric characterization was carried out for the as-fabricated back-gated devices. The channel width of the devices we studied ranges approximately from 100 to 500 μm, while the channel length ranges from 10 to 200 μm. More accurate values of the W and L used in mobility derivation are all measured via FESEM. Most devices exhibit an on-state current (I_{on}) of 1−10 μA at drain voltage of 1.0 V and gate voltage of −20 V, on/off ratio of 10^4−10^7, mobility of 10−30 $cm^2/(V\ s)$, and V_{th} of −5.0 V. Panels d−f of Figure 2 show the electric characteristics of one representative device with W = 510.5 μm and L = 88.8 μm. Figure 2g shows the plot of drain current (I_{SD}) versus gate voltage (V_G) (green curve), and the plot of divided transconductance versus V_G (blue curve). The I_{DS}−V_{DS} family curves display a clear linear regime (Figure 2e), indicating ohmic contacts formed between the silver electrodes and CNT

dx.doi.org/10.1021/nl202765b |*Nano Lett.* XXXX, XXX, 000–000

networks. Pronounced saturation behavior is observed when V_D becomes more negative, as is shown in Figure 2d. The $I_{SD}-V_G$ curves measured in the linear regime (Figure 2f) show I_{on} of 9.0 μA at V_{SD} = 0.8 V and V_G = −20 V, corresponding to a current density of 0.037 μA/μm. On/off ratio of the device is estimated to be 1.28×10^7.

We have calculated the mobility following

$$\mu = \frac{L}{W}\frac{1}{C_{ox}V_{SD}}\frac{dI_{SD}}{dV_G}$$

where L and W are the device channel length and width, V_{SD} = 1 V, the $I_{SD}-V_G$ curve is measured at V_{SD} = 1 V, and C_{ox} is the gate capacitance per unit area. If we treat the nanotube film as a uniform and continuous film, we can use a simple parallel model to calculate C_{ox}

$$C_{ox} = \frac{\varepsilon_0\varepsilon_{ox}}{t_{ox}} = 6.90 \times 10^{-9}\ \mathrm{F/cm^2}$$

given that the dielectric is 500 nm SiO_2. This results in a mobility of 23.1 $cm^2/(V\,s)$. If we consider the quantum capacitance of the nanotube network, there is a more sophisticated and rigorous model[30] to calculate C_{ox}, which gives

$$C_{ox} = \frac{D}{\frac{1}{C_{Ql}} + \frac{1}{2\pi\varepsilon_0\varepsilon_{ox}}\ln\left[\frac{\sinh(2\pi t_{ox}D)}{\pi RD}\right]}$$

where $C_{Ql} = 4 \times 10^{-10}$ F/m is the quantum capacitance of a single nanotube[30] and $D \approx 28$ tubes/μm is the nanotube density. This gives $C_{ox} = 6.74 \times 10^{-9}$ F/cm^2, which is similar to the C_{ox} value based on the parallel-plate model. This is expected as the capacitance generated by 500 nm of SiO_2 is much smaller than the quantum capacitance generated by the nanotube network. Since these two capacitances are in series, the smaller one should dominate. Hence we adopted the simple model for mobility calculation of all back-gated SWCNT TFTs.

More information can be found in Figure S2a−c in the Supporting Information about mobility, I_{on} and on/off ratio versus W and L. This study shows that these back-gated devices have relatively uniform device performance, and tunable I_{on} by designing proper W and L without compromise of mobility and on/off ratio. Overall, these as-printed SWCNT TFT devices show similar performance to their photolithography-made SWCNT TFT counterparts.[25,29]

On the basis of the measured high I_{on}, high on/off ratio, as well as high mobility of the printed SWCNT TFTs, we further explore their application in display electronics. For proof of concept, we connected an OLED to a typical SWCNT TFT back-gated device. The connection is made by putting a probe onto the drain electrode of the device, and the probe is connected to a clamp by a coaxial cable. The clamp is then fixed on the anode of the OLED. The cathode of the OLED is clamped and connected to the ground by another coaxial cable. The schematic diagram of this testing circuit is plotted in the insets of panels h and i of Figure 2. Both the device performance ($I_{SD}-V_G$ and $I_{DS}-V_{DS}$ family curves) and the OLED characterization can be found in Figure S1a-d in the Supporting Information. The OLED structure used in this study is a 4,4′-bis[*N*-(1-naphthyl)-*N*-phenylamino]biphenyl (NPD)/tris(8-hydroxyquinoline)aluminum (Alq_3) green light OLED with indium tin oxide (ITO) as the anode and aluminum (Al) as the cathode. Figure 2f shows a family of OLED current (I_{OLED}) versus V_G curves. A close

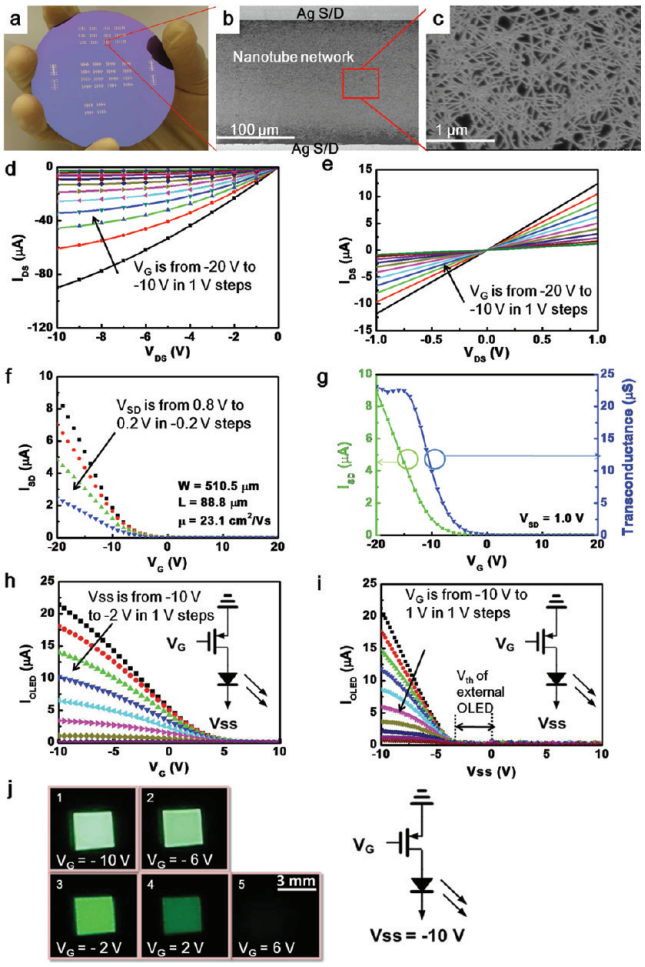

Figure 2. Characterization of fully printed back-gated SWCNT TFTs and their OLED control capability. (a−c) Optical and SEM images of fully printed back-gated SWCNT TFTs. (d, e) Output ($I_{DS}-V_{DS}$) characteristics of a representative device in saturation regime (d) and triode regime (e), respectively. (f) Transfer ($I_{SD}-V_G$) characteristics of the same device. (g) $I_{SD}-V_G$ curve (green) of the same device measured at V_{SD} = 1.0 V and its corresponding g_m-V_G curve (blue). (h, i) Electric measurement of back-gated TFT connected to an external OLED, inset shows the circuit diagram, including $I_{OLED}-V_G$ curves (f) and $I_{OLED}-V_{SS}$ curves (g). (j) Optical images showing OLED light intensity modulation through V_G of back-gated SWCNT TFT at V_{SS} = −10 V, photos numbered from 1 to 5 correspond to OLED under V_G = −10, −6, −2, 2, and 6 V, respectively. Inset shows the circuit diagram.

inspection of the curve measured at V_{SS} = −10 V and V_G = −10 V reveals that the current flowing through the OLED is 21.4 μA; when V_G = 10 V, the current flowing through the OLED is 378.0 pA. This corresponds to a modulation of I_{OLED} of 5.7×10^4. From the $I_{OLED}-V_{SS}$ curves shown in Figure 2i, good diode behavior is observed with a clear cutoff region and triode region under different V_G, showing good control from the SWCNT TFT over the OLED. The cutoff voltage of V_{SS} is around −3.5 V, in accordance with the threshold voltage of the OLED.

From the figures, the SWCNT TFT was able to provide enough driving current (21.4 μA when V_G = −10 V and V_{SS} = −10 V) for OLED, which requires around 1 μA to have observable light emission. The optical images in Figure 2j show the OLED of different light intensity under different V_G values of control SWCNT TFT, at fixed V_{SS} = −10 V. From the optical

dx.doi.org/10.1021/nl202765b |*Nano Lett.* XXXX, XXX, 000–000

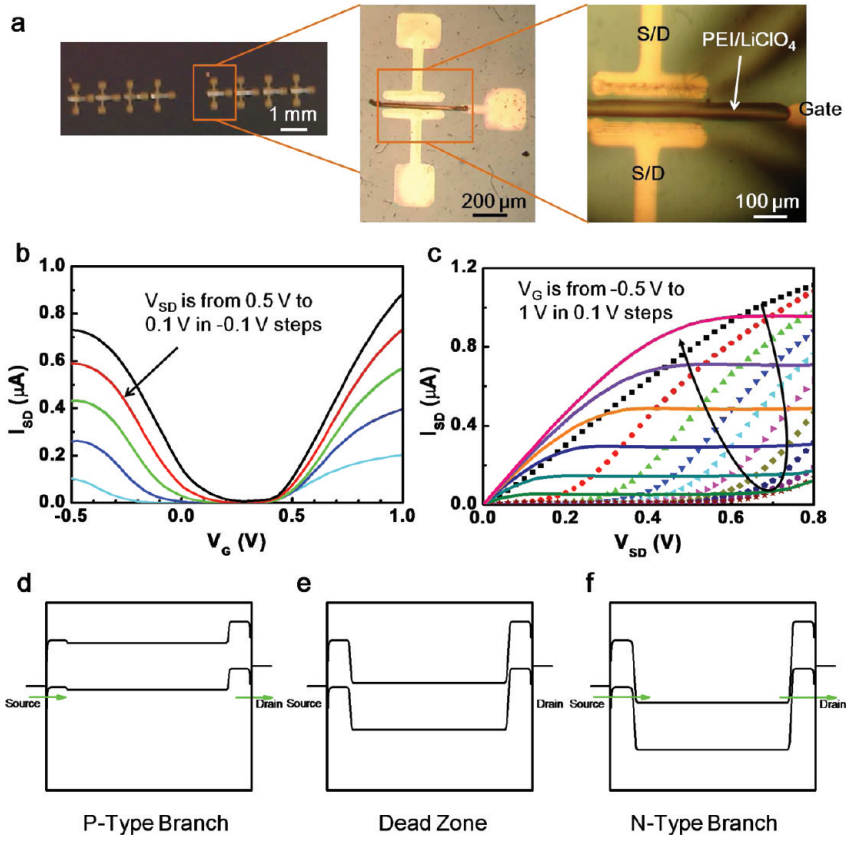

Figure 3. Characterization of fully printed top-gated SWCNT TFTs on a Si/SiO_2 wafer. (a) Optical images of fully printed top-gated SWCNT TFTs on a Si/SiO_2 wafer. (b, c) Transfer ($I_{SD}-V_G$) characteristics of one typical top-gated SWCNT TFT on a Si/SiO_2 wafer, showing ambipolar behavior. (c) Output ($I_{DS}-V_{DS}$) characteristics of the same device. (d–f) Energy band diagram of top-gated SWCNT TFTs operating in p-type branch (d), dead zone (e), and n-type branch (f).

images, the OLED is very bright when $V_G = 10$ V, gets dimmed as V_G increases positively, and is totally turned off when V_G becomes more positive (6 V), corresponding to the $I_{OLED}-V_G$ curve measured at $V_{SS} = -10$ V in Figure 2h, where the curve enters the cutoff region around 5.5 V.

This single transistor used in the above OLED control test can be viewed as a modified control circuit shown in Figure 1a. The next step is to realize the more complicated display control circuit shown in Figure 1b, which allows longer storage time than the circuit in Figure 1a. The easiest way is to fabricate top gate SWCNT TFTs based on the back-gated TFTs we have printed. Here we used PEI (M_w: 10k, Sigma Aldrich) as ion gel dielectric for SWCNT TFTs. Due to the large molecular weight, pure PEI has a high viscosity and therefore is unable to print out. Here we dissolve PEI in methanol in 1:5 volume ratio, and then stir for overnight to reduce the viscosity before printing. Besides, to improve the gate conductance, a small amount of $LiClO_4$ ($LiClO_4$ to PEI weight ratio: 1–2.5) is added to fine-tune the device performance. Figure 3a shows the optical images of arrays of top-gated SWCNT TFTs, a top-gated SWCNT TFT, and a zoomed-in image of the channel region, respectively. The fully printed top-gated SWCNT TFTs were characterized by electric measurement in ambient air. Interestingly, ambipolar behavior was observed for most devices. Panels b and c of Figure 3 show the $I_{SD}-V_G$ and $I_{SD}-V_{SD}$ curves of a typical ambipolar device. This is different from what was reported in the literature,[31−34] where n-type SWCNT transistors were obtained when pure PEI or PEI/$LiClO_4$ was spin coated to cover the whole device and used as the ion gel dielectric. Here we notice that the coverage of our fully printed SWCNT TFT is different from literature, and it may explain what we observed. From the optical image in Figure 3a, only part of the channel is covered with PEI/$LiClO_4$ and part of the channel is exposed to air, while in literature,[31−34] the channel region of CNT devices is fully covered with spin-coated PEI/$LiClO_4$. SWCNT TFTs are p-type in ambient air because the oxygen molecules adsorbed onto nanotubes can act as electron acceptors. However, it has been reported that the carrier type in SWCNTs can be modified by introducing electron donors or acceptors. PEI/$LiClO_4$ is known to change the carrier type of CNT from p-type to n-type, because the oxygen atom in PEI/$LiClO_4$ can be adsorbed onto the SWNT sidewall and act as electron donors to compensate for the p-type doping effect from the oxygen molecules. If the PEI/$LiClO_4$ coverage is 100%, then the whole channel region would become n-type, and the devices would assume exclusively n-type behavior. However, if only the middle part of the channel region is covered by PEI/$LiClO_4$, then only the middle part of the channel becomes n-type doped while the uncovered regions still remain p-type. Such a doping condition may induce band-to-band (BTB) tunneling[35] under certain biasing conditions while operating as a MOSFET under some other biasing condition, showing ambipolar behavior in $I_{SD}-V_G$ curves. We also notice that the coverage of PEI/$LiClO_4$ needs to be beyond a certain point to reduce the tunneling distance so as to favor BTB tunneling, or the device would become very resistive after PEI printing.

dx.doi.org/10.1021/nl202765b |*Nano Lett.* XXXX, XXX, 000–000

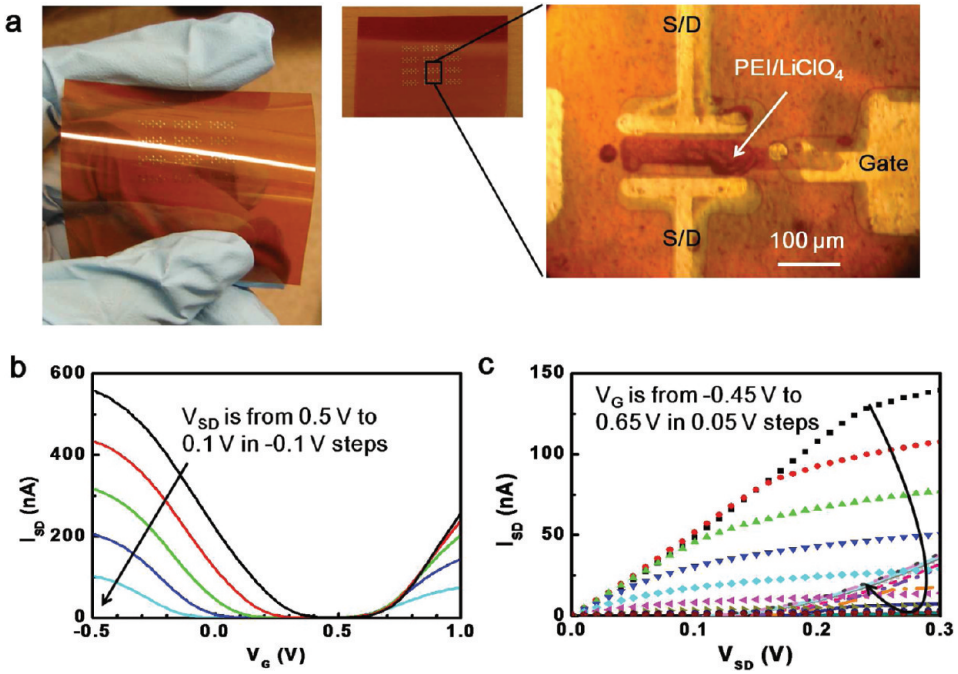

Figure 4. Characterization of fully printed top-gated SWCNT TFTs on Kapton. (a) Optical images of top-gated SWCNT TFTs printed on Kapton. (b) Transfer ($I_{SD}-V_G$) characteristics of one typical top-gated SWCNT TFT on Kapton with ambipolar behavior. (c) Output ($I_{DS}-V_{DS}$) characteristics of the same device.

Such carrier type modulation via the coverage of PEI/$LiClO_4$ of these fully printed top-gated devices could be more clearly explained by the energy band diagrams. Figure 3d−f shows the energy band structure of p-type conduction, a dead zone with little conduction, and n-type conduction due to BTB tunneling. The green arrows denote which type of carrier is favored. When V_G is negative, both the ungated and gated nanotube sections are p-type, and holes can flow from source to drain, therefore leading to p-type conduction (Figure 3d). As V_G increases positively, the gated nanotube would become gradually n-type, while the ungated nanotubes remain p-type, resulting in the nonconductive dead zone (Figure 3e). However, as V_G becomes even more positive, the tunneling barrier between the p-type region and the n-type region becomes very thin, thereby favoring BTB tunneling current (Figure 3f).

Besides conduction mechanism, other important electrical characteristics are subthreshold slope and mobility. From Figure 3b, the subthreshold swings of the ambipolar top-gated device are calculated to be 258 mV/decade for p-type branch and 136 mV/decade for n-type branch. Mobility calculation for a polymer-gated device requires more analysis of total gate capacitance. From ref 33, the capacitance provided by PEI/$LiClO_4$ polymer should be

$$C_{PG} = \frac{\varepsilon\varepsilon_0}{\lambda}$$

where λ is the Debye length calculated by

$$\lambda = \sqrt{\frac{\varepsilon\varepsilon_0 kT}{2\rho e^2}}$$

Here, ρ is the concentration of $LiClO_4$, $\varepsilon = 10$ is the dielectric constant of PEI. The calculated value for C_{PG} is 2.062×10^{-3} F/cm^2. Quantum capacitance generated by a carbon nanotube network is quantified by

$$C_Q = C_{Ql}D = 1.12 \times 10^{-6}\ \text{F/cm}^2$$

For nanotubes gated by PEI/$LiClO_4$, the nanotube quantum capacitance and the polymer gate capacitance would be in series, and thereby the nanotube quantum capacitance would dominate, which is almost 10^3 times smaller than that of PEI/$LiClO_4$. On the basis of this, the calculated mobility for holes of the ambipolar top-gated transistor is about 0.42 cm^2/(V s) and the calculated mobility for electrons is about 0.56 cm^2/(V s). Compared to the back-gated devices, the polymer gated transistors have much lower mobility. This is not surprising as there would be more scattering at a nanotube/polymer gate interface, which impedes carrier transportation. However, due to the high gate capacitance provided by the quantum capacitance of CNTs, the transistor itself still can provide an on-state current density of 0.002 μA/μm at $V_G = 1$ V and $V_{DS} = 0.5$ V, which would be sufficient to drive the OLED.

As a proof of concept, we also printed top-gated SWCNT TFTs on Kapton to demonstrate a fully printed flexible device. Figure 4a shows the optical images of an array of fully printed top-gated SWCNT TFTs on Kapton, including a zoomed-in image which clearly shows the PEI/$LiClO_4$ gate covers the middle region of the source and drain, leaving a gap near the source and drain electrode, respectively. Electric measurement of devices on Kapton and Si/SiO_2 shows no significant differences. Device performances of a representative top-gated device on Kapton are plotted in panels b and c of Figure 4. For this device, ambipolar behavior dominates and it is consistent with the above explanation, although the n-type branch is very weak and the MOSFET-like behavior is hard to observe. The calculated hole mobility is about 0.86 cm^2/(V s) and the calculated electron mobility is about 0.90 cm^2/(V s). The subthreshold swings are about 80 mV/decade for the p-type branch and 97.5 mV/decade

dx.doi.org/10.1021/nl202765b |*Nano Lett.* XXXX, XXX, 000–000

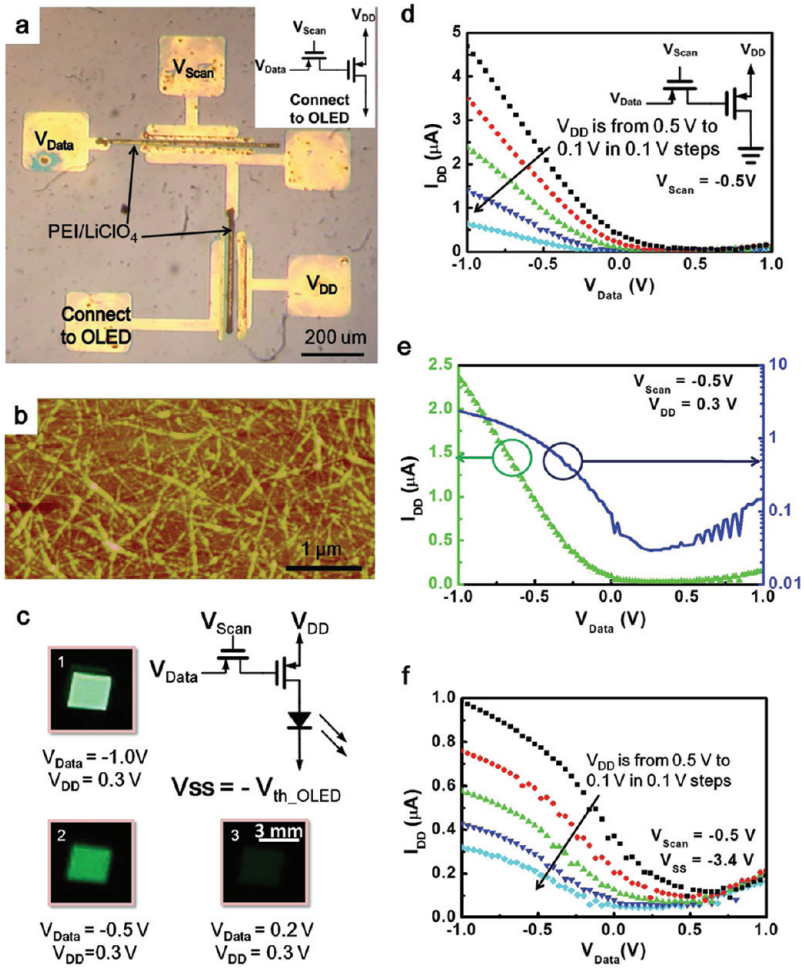

Figure 5. Characterization of the 2T control circuit made of two fully printed top-gated SWCNT TFTs. (a) Optical image of one 2T OLED display control circuit, inset shows corresponding circuit diagram. (b) AFM image of channel region of the transistors in 2T OLED display control circuit before $PEI/LiClO_4$ printing. (c) Optical images taken at $V_{Data} = -1.0$ V (1), -0.5 V (2), and 0.2 V (3), respectively. V_{DD} is 0.3 V and V_{Scan} is -0.5 V. (d, e) Characterization of 2T control circuit alone, including $I_{DD}-V_{Data}$ curves (d), and one $I_{DD}-V_{Data}$ curve in both linear plot (green) and log plot (blue) (e).(f) $I_{DD}-V_{Data}$ curves of 2T control circuit connected to external OLED.

for the n-type branch. The on-state current density is about 0.001 $\mu A/\mu m$.

We have also compared the hysteresis of all the devices mentioned above: back-gated devices on silicon wafers, top-gated ambipolar devices on Kapton, and top-gated ambipolar devices on Si/SiO_2 wafers. This piece of information can be found in Figure S3a−c in the Supporting Information. Hysteresis of top-gated devices is very small, compared to that of the back-gated devices, probably due to stronger gating effect offered by the top gate. We demonstrated a simple inverter function by using two fully printed top-gated transistors. Additional information can be found in Figure 4 in the Supporting Information.

Stability is an important issue in commercialization of any useful technology. For AMOLED applications, we envision that the printed carbon nanotube transistors will be fully integrated with OLED arrays, and the encapsulation technology developed for OLEDs will also keep the CNT transistors well protected, as the organics in OLEDs are very sensitive to oxygen and moisture. Thereby OLEDs, instead of CNT transistors, would set the lifetime of the AMOLED display. Regarding printed CNT transistors without encapsulation, while CNTs and silver electrodes are stable in air, a typical lifetime of $PEI/LiClO_4$ in air is reported to be at least several weeks.[33] As mentioned above, proper encapsulation can mitigate and eliminate the stability problem.

Study of how the $PEI/LiClO_4$ operates as gate dielectric for SWCNT TFTs paves the way for 2T1C OLED control circuit. For demonstration purpose, we omitted the storage capacitance and tested the transistor-only (2T) OLED control circuit. The photograph of the fully printed 2T OLED display circuit is shown in Figure 5a, and the inset shows the equivalent schematic circuit diagram of this as-fabricated circuit. The atomic force microscopy (AFM) image shown in Figure 5b is taken before $PEI/LiClO_4$ printing, confirming that the carbon nanotube density of this device is very high. Electric property characterizations were done first without the OLED, as indicated in the circuit diagram shown in the inset of Figure 5d. With V_{DD} biased at 0.1 , 0.2 , 0.3 , 0.4, and 0.5 V and V_{Data} swept from -1 to 1 V, when $V_{Scan} = 0$ V, the switch transistor is cut off and there is no current through the driving transistor. When $V_{Scan} = -0.5$ V, the switch transistor turns on and it passes V_{Data} to the driving transistor. The details of how V_{Data} controls the current provided by the driving transistor (I_{DD}) are plotted in Figure 5d, under different V_{DD} ranging from 0.5 to 0.1 V. Specifically, the $I_{DD}-V_{Data}$ curve measured under $V_{DD} = 0.3$ V is magnified and replotted in Figure 5e, in both linear and log scales.

dx.doi.org/10.1021/nl202765b |*Nano Lett.* XXXX, XXX, 000–000

Subsequently, an external OLED is directly connected to this display circuit, with the cathode connected to the drain of the driving transistor and anode connected to a negative voltage of −3.4 V, which is used to provide the voltage drop on OLED in on state. The connections are made via probes and coaxial cables with clamps in a way similar to connecting an external OLED to a single device, which has been described. $I_{DD}-V_{Data}$ was measured at V_{DD} = 0.1, 0.2, 0.3, 0.4, and 0.5 V (Figure 5f). Modulation of the OLED light output can be clearly observed, and the optical images in Figure 5c numbered 1, 2, 3 were taken under V_{Data} = −1.0, −0.5, and 0.2 V, respectively, when V_{DD} = −0.3 V.

In addition, we carried out frequency investigation of single top-gated and back-gated transistors. This study is included in Figure S5a−d in the Supporting Information. The 3 dB frequency is found to be 5.66 kHz for back-gated SWCNT TFT and 93.3 Hz for top-gated SWCNT TFT.

In summary, we have successfully fabricated fully printed SWCNT TFT circuits for OLED control and display. The back-gated printed transistors are made of 98% semiconducting SWCNTs as the channel and printed Ag nanoparticles as electrodes, and they exhibit good mobility (10−30 cm^2/(V s)), good on/off ratio (10^4−10^7), and good current carrying capacity. They are ideal components for OLED-based display backplane electronics, and the control over external OLED using one single back-gated SWCNT TFT is demonstrated. In addition, with one more printing step of PEI/$LiClO_4$, these back-gated SWCNT TFTs are converted to top-gated SWCNT TFTs with ambipolar behavior. Furthermore, top-gated SWCNT TFTs are also made on Kapton to demonstrate the potential of using this technology for flexible electronics. Finally, a two-transistor OLED control circuit composed of two fully printed top-gated SWCNT TFTs is made and its ability to control over external OLED is demonstrated. Our work shows the great potential of printed electronics based on semiconducting carbon nanotubes as a cost-effective and scalable approach for display backplane electronics (OLED and LCD) and other macroelectronics applications.

■ ASSOCIATED CONTENT

Supporting Information. Electric properties of the external OLED and the control device used in Figure 2 (S1), statistic study of I_{on}, mobilities, and on/off ratio of the fully printed back-gated SWCNT TFTs (S2), hysteresis of the fully printed back-gated and top-gated devices (S3), electric properties of the inverter composed of two top-gated devices (S4), and frequency study of the fully printed back-gated and top-gated devices (S5). This material is available free of charge via the Internet at http://pubs.acs.org.

■ AUTHOR INFORMATION

Corresponding Author

*E-mail: kos@ee.ucla.edu, chongwuz@usc.edu.

Author Contributions

‖These authors contributed equally to this work.

■ ACKNOWLEDGMENT

We acknowledge financial support by a DARPA SBIR Contract (HR 0011-10-0-0003) and Defense Threat Reduction Agency (HDTRA1-10-1-0015). We thank Dr. Todd Hylton from the Defense Science Office of DARPAR for helpful suggestions. We thank Professor Mark Hersam of Northwestern University and Mr. Elliott Garlock and Dr. Nathan Yoder of Nanointegris for valuable discussions.

■ REFERENCES

(1) Heilmeie, G. H.; Castella, J. A.; Zanoni, L. A. *Mol. Cryst. Liq. Cryst.* **1969**, *8*, 293–304.
(2) Heilmeie, G. H.; Zanoni, L. A.; Barton, L. A. *Pr. Inst. Electr. Elect.* **1968**, *56*, 1162–1171.
(3) Tang, C. W.; Vanslyke, S. A. *Appl. Phys. Lett.* **1987**, *51*, 913–915.
(4) Nusca, Andrew Amazing: Sony's paper-thin 'rollable' flexible OLED display. *ZDNet* (May 26, 2010). Retrieved July 26, 2011 from http://www.zdnet.com/blog/gadgetreviews/amazing-sonys-paper-thin-rollable-flexible-oled-display/15136.
(5) Rogers, J. A.; Bao, Z.; Baldwin, K.; Dodabalapur, A.; Crone, B.; Raju, V. R.; Kuck, V.; Katz, H.; Amundson, K.; Ewing, J.; Drzaic, P. *Proc. Natl. Acad. Sci. U.S.A.* **2001**, *98*, 4835–4840.
(6) Bao, Z. N.; Feng, Y.; Dodabalapur, A.; Raju, V. R.; Lovinger, A. *J. Chem. Mater.* **1997**, *9*, 1299–&.
(7) Liu, Y.; Cui, T. H. *Macromol. Rapid Commun.* **2005**, *26*, 289–292.
(8) Cho, J. H.; Lee, J.; Xia, Y.; Kim, B.; He, Y. Y.; Renn, M. J.; Lodge, T. P.; Frisbie, C. D. *Nat. Mater.* **2008**, *7*, 900–906.
(9) Liu, Y.; Cui, T. H.; Varahramyan, K. *Solid-State Electron.* **2003**, *47*, 1543–1548.
(10) Chen, B.; Cui, T. H.; Liu, Y.; Varahramyan, K. *Solid-State Electron.* **2003**, *47*, 841–847.
(11) Liu, Y.; Varahramyan, K.; Cui, T. H. *Macromol. Rapid Commun.* **2005**, *26*, 1955–1959.
(12) Rogers, J. A.; Bao, Z. N.; Dodabalapur, A.; Makhija, A. *IEEE Electron Device Lett.* **2000**, *21*, 100–103.
(13) Javey, A.; Guo, J.; Wang, Q.; Lundstrom, M.; Dai, H. J. *Nature* **2003**, *424*, 654–657.
(14) Durkop, T.; Getty, S. A.; Cobas, E.; Fuhrer, M. S. *Nano Lett.* **2004**, *4*, 35–39.
(15) Kang, S. J.; Kocabas, C.; Ozel, T.; Shim, M.; Pimparkar, N.; Alam, M. A.; Rotkin, S. V.; Rogers, J. A. *Nat. Nanotechnol.* **2007**, *2*, 230–236.
(16) Kong, J.; Franklin, N. R.; Zhou, C.; Chapline, M. G.; Peng, S.; Cho, K.; Dai, H. *Science* **2000**, *287*, 622.
(17) Ishikawa, F. N.; Curreli, M.; Olson, C. A.; Liao, H.-I.; Sun, R.; Roberts, R. W.; Cote, R. J.; Thompson, M. E.; Zhou, C. *ACS Nano* **2010**, *4*, 6914–6922.
(18) Ishikawa, F. N.; Stauffer, B.; Caron, D. A.; Zhou, C. *Biosens. Bioelectron.* **2009**, *24*, 2967–2972.
(19) Barone, P. W.; Baik, S.; Heller, D. A.; Strano, M. S. *Nat. Mater.* **2005**, *4*, 86–92.
(20) Cao, Q.; Kim, H. S.; Pimparkar, N.; Kulkarni, J. P.; Wang, C. J.; Shim, M.; Roy, K.; Alam, M. A.; Rogers, J. A. *Nature* **2008**, *454*, 495–500.
(21) Javey, A.; Wang, Q.; Ural, A.; Li, Y. M.; Dai, H. J. *Nano Lett.* **2002**, *2*, 929–932.
(22) Bachtold, A.; Hadley, P.; Nakanishi, T.; Dekker, C. *Science* **2001**, *294*, 1317–1320.
(23) Chen, Z. H.; Appenzeller, J.; Lin, Y. M.; Sippel-Oakley, J.; Rinzler, A. G.; Tang, J. Y.; Wind, S. J.; Solomon, P. M.; Avouris, P. *Science* **2006**, *311*, 1735–1735.
(24) Sun, D.-m.; Timmermans, M. Y.; Tian, Y.; Nasibulin, A. G.; Kauppinen, E. I.; Kishimoto, S.; Mizutani, T.; Ohno, Y. *Nat. Nanotechnol.* **2011**, *6*, 156–161.
(25) Wang, C.; Zhang, J. L.; Ryu, K. M.; Badmaev, A.; De Arco, L. G.; Zhou, C. W. *Nano Lett.* **2009**, *9*, 4285–4291.
(26) Ishikawa, F. N.; Chang, H. K.; Ryu, K.; Chen, P. C.; Badmaev, A.; De Arco, L. G.; Shen, G. Z.; Zhou, C. W. *ACS Nano* **2009**, *3*, 73–79.
(27) Tsukada, T. *TFT/LCD Liquid-Crystal Displays Addressed by Thin-Film Transistors*; Gordon and Breach Publishers: Austrailia, 1994; Vol. 29, p 193.

(28) Chen, P. C.; Shen, G. Z.; Chen, H. T.; Ha, Y. G.; Wu, C.; Sukcharoenchoke, S.; Fu, Y.; Liu, J.; Facchetti, A.; Marks, T. J.; Thompson, M. E.; Zhou, C. W. *ACS Nano* **2009**, *3*, 3383–3390.
(29) Wang, C.; Zhang, J. L.; Zhou, C. W. *ACS Nano* **2010**, *4*, 7123–7132.
(30) Cao, Q.; Xia, M. G.; Kocabas, C.; Shim, M.; Rogers, J. A. *Appl. Phys. Lett.* **2007**, *90*, 023516.
(31) Shim, M.; Javey, A.; Kam, N. W. S.; Dai, H. J. *J. Am. Chem. Soc.* **2001**, *123*, 11512–11513.
(32) Lu, C. G.; Fu, Q.; Huang, S. M.; Liu, J. *Nano Lett.* **2004**, *4*, 623–627.
(33) Siddons, G. P.; Merchin, D.; Back, J. H.; Jeong, J. K.; Shim, M. *Nano Lett.* **2004**, *4*, 927–931.
(34) Ozel, T.; Gaur, A.; Rogers, J. A.; Shim, M. *Nano Lett.* **2005**, *5*, 905–911.
(35) Appenzeller, J.; Lin, Y. M.; Knoch, J.; Avouris, Ph. *Phys. Rev. Lett.* **2004**, *93*, 196805.

dx.doi.org/10.1021/nl202765b |*Nano Lett.* XXXX, XXX, 000–000